Acta Crystallographica Section A
Foundations of Crystallography
ISSN 0108-7673

Received 20 March 2001
Accepted 14 May 2001

The structure of a decagonal $Al_{72}Ni_{20}Co_8$ quasicrystal

Hiroyuki Takakura,[a]*† Akiji Yamamoto[b]† and An Pang Tsai[c]‡

[a]CREST, Japan Science and Technology Corporation and National Research Institute for Metals, Tsukuba 305-0047, Japan, [b]National Institute for Research in Inorganic Materials, Tsukuba 305-0044, Japan, and [c]National Research Institute for Metals, Tsukuba 305-0047, Japan. Correspondence e-mail: takakura@tamamori.nims.go.jp

The structure of a decagonal $Al_{72}Ni_{20}Co_8$ quasicrystal with space group $P10_5/mmc$ has been determined on the basis of a single-crystal X-ray data set using the five-dimensional description. The best-fit model structure based on a cluster model having lower symmetry than the decagonal symmetry with 103 parameters gives $wR = 0.045$ and $R = 0.063$ for 449 reflections. The structure is well described by the hexagon, boat and star tiling with an edge length of 6.36 Å and is very consistent with recent high-resolution electron-microscopy images. The refined structure is compared with previously discussed model structures including cluster-based models having 20 Å tenfold symmetric clusters.

1. Introduction

Just after the discovery of icosahedral quasicrystals (Shechtman *et al.*, 1984), decagonal quasicrystals were found in Al–Mn alloy (Bendersky, 1985; Chattopadhyay *et al.*, 1985). The decagonal quasicrystals have unique structural characteristics, since they have periodicity in one direction, the *c* axis, and quasiperiodicity in a plane perpendicular to it. Nowadays, several stable decagonal quasicrystals have been found in different kinds of alloy systems: Al–Pd–Mn, Al–Pd–TM (TM = Fe, Ru and Os), Al–Cu–Co, Al–Ni–Co and Zn–Mg–RE (RE = Y, Dy, Ho, Lu, Tb and Gd) (Tsai, 1999). They show various periods along the *c* axis: 4, 8, 12 or 16 Å. Among them, Al–Ni–Co decagonal quasicrystals (Tsai *et al.*, 1989) have been extensively studied by various experimental techniques as shown below, although the detailed atomic structure is still under discussion.

The phase diagram of Al–Ni–Co has already been extensively studied (Gödecke & Ellner, 1996, 1997; Scheffer *et al.*, 1998). It has been found that there are several variant structures in this decagonal phase which are strongly dependent on both temperature and chemical composition (Ritsch *et al.*, 1998). The one basic and seven variant structures were exemplified in the stable decagonal Al–Ni–Co quasicrystals, including three superstructure phases: the type I superstructure (S1 + S2) discovered by Edagawa *et al.* (1992), its high-temperature modification, S1 (Edagawa *et al.*, 1994), and the type II superstructure (Ritsch *et al.*, 1995). Those variant structures usually show diffuse scattering layers perpendicular to the c^* axis, which imply some disorder related to an 8 Å period (Frey *et al.*, 2000). In an early stage, two Al–Ni–Co decagonal quasicrystals have been investigated by means of X-ray structure analysis: $Al_{70}Ni_{10}Co_{20}$ (Yamamoto *et al.*, 1990) and $Al_{70}Ni_{15}Co_{15}$ (Steurer *et al.*, 1993). It is understood that both phases are classified in the variant structures at present. Indeed, in their analyses, imperfections of the structures mentioned above were ignored. High-resolution transmission-electron-microscopy (HRTEM) images with such variant structures usually show a tenfold cluster symmetry (Hiraga *et al.*, 1991). This led to an established consensus that a 20 Å cluster should have perfect tenfold symmetry and this is the building unit of the decagonal quasicrystals.

On the other hand, one can obtain a highly perfect basic phase of the decagonal Al–Ni–Co quasicrystals (Ritsch *et al.*, 1996; Tsai *et al.*, 1996). The representative of this ideal phase has a composition $Al_{72}Ni_{20}Co_8$, which shows neither diffuse scattering nor superlattice reflections (Tsai *et al.*, 1996). Moreover, this phase has the shortest period of 4 Å along the *c* axis among the decagonal quasicrystals. This suggests that the ideal phase is highly homogeneous and has a simple atomic structure. Therefore, the $Al_{72}Ni_{20}Co_8$ compound is the best candidate for investigating its detailed atomic structure. This ideal phase, however, has only been investigated so far by electron diffraction or microscopy techniques (Ritsch *et al.*, 1996; Saitoh *et al.*, 1997; Yan *et al.*, 1998; Abe *et al.*, 2000). A new experimental technique called the high-angle annular dark-field (HAADF) method has been applied for the first time to decagonal $Al_{72}Ni_{20}Co_8$ quasicrystals by Saitoh *et al.* (1997). The high-resolution images recorded using this new technique clearly showed the transition-metal atom positions (Saitoh *et al.*, 1997; Yan *et al.*, 1998). The images strongly suggested that symmetry breaking of so-called 20 Å tenfold symmetric clusters (Hiraga *et al.*, 1991) occurs in the basic phase (Saitoh *et al.*, 1997; Yan *et al.*, 1998). A structure model for this phase has been proposed on the basis of the local structure of the $Al_{13}Fe_4$ monoclinic phase (Black, 1955*a*;

† Present affiliation: Advanced Materials Laboratory, National Institute for Materials Science, Tsukuba 305-0044, Japan.
‡ Present affiliation: Materials Engineering Laboratory, National Institute for Materials Science, Tsukuba 305-0047, Japan.

Saitoh *et al.*, 1998). Another structure model based on the often-discussed Burkov model (Burkov, 1991) has also been proposed for the same material (Yan *et al.*, 1998). Meanwhile, in response to this new experimental evidence, a quite conceptually different model based on the Gummelt prototile decagon (Gummelt, 1996) has been presented (Steinhardt *et al.*, 1998; Abe *et al.*, 2000). Further, a structure model for decagonal Al–Cu–Co quasicrystals has been proposed recently based on Monte Carlo simulations (Cockayne & Widom, 1998). Owing to the universality of the employed basic structure, the Penrose tiling, the model can also be considered as a structure model of the decagonal Al–Ni–Co quasicrystals. Therefore, there are several competitive structure models for the decagonal $Al_{72}Ni_{20}Co_8$ quasicrystal. These require a detailed experimental examination. Recently, a comparison of experimental images of the decagonal $Al_{72}Ni_{20}Co_8$ quasicrystal and the model by Cockayne & Widom (1998) have been published (Wittmann, 1999).

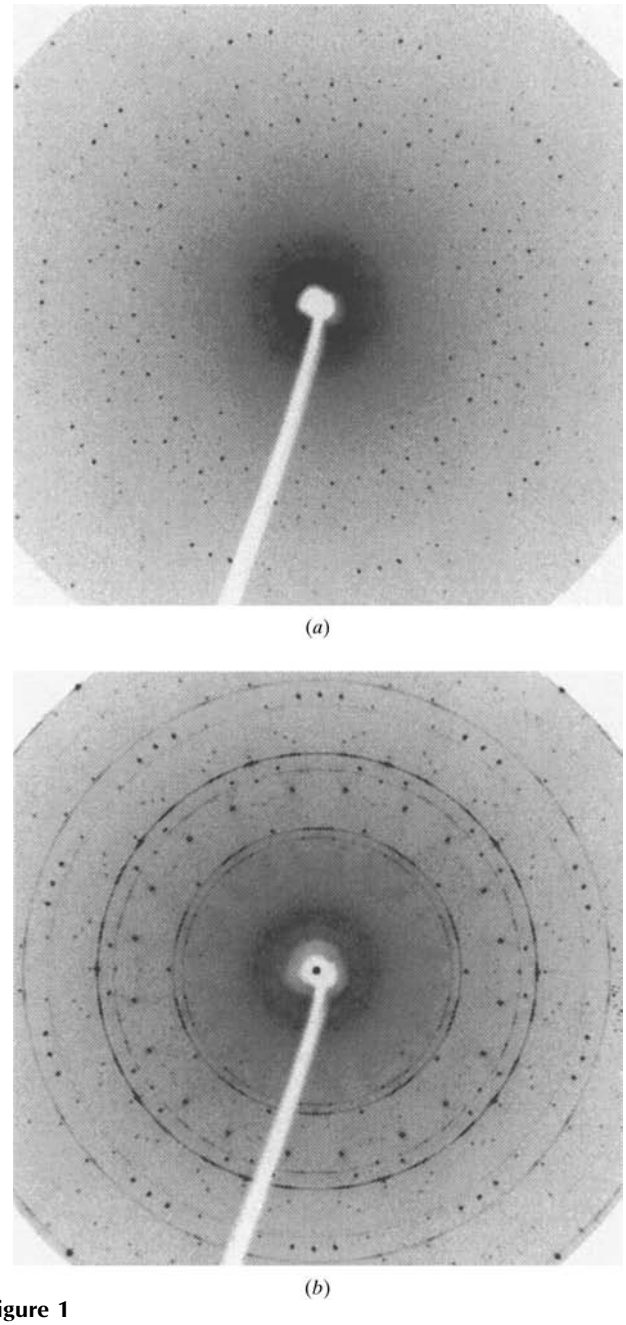

Figure 1
Transmission Laue photographs taken along the tenfold axis for (*a*) $Al_{72}Ni_{20}Co_8$ and (*b*) $Al_{72}Ni_{12}Co_{16}$. Note that $Al_{72}Ni_{20}Co_8$ does not show any circular diffuse scattering from the diffuse layers perpendicular to the c^* axis. The diffuse hump close to the origin in both photographs is due to air scattering.

Structure refinement methods of quasicrystals have not been established yet because of the complexity in their structures. A basic problem is how to introduce positional parameters to describe the structure in detail. Here we employ a cluster model in a higher-dimensional space (Yamamoto *et al.*, 1994; Yamamoto, 1996). In this model, a large occupation domain in the internal (complementary) space is divided into several subdomains and each subdomain generates atoms in the external (physical) space which are located in a similar local environment. Therefore, we can assume that such atoms have the same atomic displacement parameter and occupation probability. Moreover, positional parameters can be introduced to represent shifts from their ideal positions. This refinement method has been applied to an icosahedral Al–Pd–Mn quasicrystal (Yamamoto *et al.*, 1994) as well as to a decagonal Al–Pd–Mn quasicrystal (Weber & Yamamoto, 1997, 1998). It has been confirmed that the refinement of the atom shifts from their ideal positions and the use of the subdividable occupation domains are crucial to improve the fitting results. In the above examples, however, the subdivision of large occupation domains was based on a cluster having the same symmetry with that of the global symmetry of quasicrystals, *i.e.* icosahedral or decagonal symmetry. In this paper, we perform a detailed structure analysis of the decagonal $Al_{72}Ni_{20}Co_8$ quasicrystal based on the X-ray diffraction technique for the first time, where the subdivision scheme employed does not assume the decagonal cluster. This provides several improvements over the results of the former analysis of decagonal Al–Ni–Co quasicrystals. The obtained best-fit model is well described by the hexagon, boat and star (HBS) tiling with an edge length of 6.36 Å. On the basis of this refined structure model, the reported electron-microscopy images of $Al_{72}Ni_{20}Co_8$ are re-interpreted.

The arrangement of the paper is as follows. In §2, we describe the experimental details. In §3, we construct an initial structure model for the decagonal Al–Ni–Co quasicrystals. We perform the structure refinement and give the results in §4, and in §5 the real-space structure derived from the refined model is described in detail. In §6, we discuss the implications of the refined structure and compare it with previous models, and the final section is dedicated to conclusions.

2. Experimental details

2.1. Sample preparation

An alloy of nominal composition $Al_{72}Ni_{20}Co_8$ was melted in an Ar atmosphere, annealed at a temperature of 1373 K for 1 h and 1173 K for 60 h, then quenched into cold water. The

measured atomic density of the present sample is D_x = 3.94 Mg m^{-3}. Any deviation from an initial composition $Al_{72}Ni_{20}Co_8$ was not observed within experimental error. The sample, about 0.2 mm in diameter and 0.28 mm in length, having an ellipsoid shape, after polishing a single crystal showing a decagonal prismatic habit, was used for subsequent X-ray diffraction experiments.

2.2. Laue photographs

The sample quality and the amount of the diffuse scattering phenomena were checked by using X-ray Laue and oscillation techniques. As an example, the X-ray transmission Laue photograph of the present sample taken along an incident beam parallel to the tenfold axis is displayed in Fig. 1 together with that obtained from a sample having a different composition, $Al_{72}Ni_{12}Co_{16}$, for the sake of comparison. These photographs were taken using Mo radiation from a rotating-anode X-ray generator operated at 40 kV and 50 mA. The exposure time was 5 min. As a recording medium, a flat FUJI-BAS-SR2040 imaging plate was utilized. We see only sharp Bragg spots having tenfold symmetry in Fig. 1(*a*), while additional concentric rings are observed in Fig. 1(*b*). These concentric rings are circular segments of the diffuse layers, which are observed as a result of intersections of the Ewald spheres by characteristic Mo $K\alpha$ and $K\beta$ X-rays, and the diffuse layers perpendicular to the tenfold axis. These concentric rings are always observed if there are diffuse scattering layers coming from some disorder related to an 8 Å period along the c axis as in $Al_{72}Ni_{12}Co_{16}$. From these preliminary X-ray diffraction experiments, it was confirmed that unnecessary disorder is quite small in the present sample. Therefore, it was concluded that the quality of the sample is suitable for performing an X-ray structure analysis.

2.3. Decagonal coordinate system

The five basic vectors for a decagonal quasicrystal in the reciprocal space which are necessary for indexing are defined as

$$\mathbf{d}_i^* = \sum_j \tilde{M}_{ij}^{-1}\mathbf{a}_j$$

with

$$\tilde{M}^{-1} = \frac{a^*}{5^{1/2}}\begin{bmatrix} c_1 & s_1 & c_2 & s_2 & 0 \\ c_2 & s_2 & c_4 & s_4 & 0 \\ c_3 & s_3 & c_1 & s_1 & 0 \\ c_4 & s_4 & c_3 & s_3 & 0 \\ 0 & 0 & 0 & 0 & 5^{1/2}c^*/a^* \end{bmatrix}, \qquad (1)$$

where $\mathbf{a}_j$ (j = 1, 2, ..., 5) are the orthogonal unit-length vectors. $\mathbf{a}_1$, $\mathbf{a}_2$ and $\mathbf{a}_5$ are taken in the external space and $\mathbf{a}_3$, $\mathbf{a}_4$ in the internal space. The tilde denotes a transpose of the matrix and $c_j = \cos(2\pi j/5)$, $s_j = \sin(2\pi j/5)$ (j = 1, 2, 3, 4), while a^* and c^* are the reciprocal-lattice constants.

The corresponding unit vectors in the direct space are given by

$$\mathbf{d}_i = \sum_j M_{ij}\,\mathbf{a}_j.$$

The matrix M is written as

$$M = \frac{2a}{5^{1/2}}\begin{bmatrix} c_1-1 & s_1 & c_2-1 & s_2 & 0 \\ c_2-1 & s_2 & c_4-1 & s_4 & 0 \\ c_3-1 & s_3 & c_1-1 & s_1 & 0 \\ c_4-1 & s_4 & c_3-1 & s_3 & 0 \\ 0 & 0 & 0 & 0 & 5^{1/2}c/2a \end{bmatrix}, \qquad (2)$$

where $a = 1/a^*$ and $c = 1/c^*$ are what we call decagonal lattice constants.

This coordinate system is the same as that of our previous paper (Yamamoto & Ishihara, 1988), but different from those of Steurer *et al.* (1993) and Cockayne & Widom (1998).

2.4. Intensity data collection

Single-crystal X-ray diffraction measurements were carried out on an Enraf–Nonius CAD-4 four-circle diffractometer equipped with graphite monochromator (Mo $K\alpha$ radiation, λ = 0.7107 Å). The lattice constants were refined to be a = 2.719 and c = 4.090 Å with 25 selected reflections. Intensity data were measured using the 2θ–ω scan mode at 6751 pre-calculated reflection positions that belong to the tripled asymmetric regions ($2 \le \theta \le 35^\circ$) in the reciprocal space with the five-dimensional generalized Miller indices $-6 \le h_i \le 6$ (i = 1, 2, 3, 4) and $0 \le h_5 \le 6$. The index of the strongest reflection in the zeroth layer is 13420. After performing Lorentz and polarization corrections, 615 unique reflections were obtained by averaging ($R_{\rm int}$ = 0.034, $R_{\rm int} = \sum ||F_o| - \langle F_o\rangle|/\sum |F_o|$) and 451 unique reflections [$|F_o| > 3\sigma(|F_o|)$] were used in the analysis. A numerical absorption correction for an ellipsoid sample was applied within a least-squares program, where the linear absorption coefficient μ = 9.356 mm^{-1} was calculated from the mass absorption coefficients μ_k/ρ of the elements (*International Tables for X-ray Crystallography*, 1962, Vol. III).

From the systematic extinctions ($h_1\bar{h}_2\bar{h}_2h_1h_5$ with h_5 = $2n+1$ and $0000h_5$ with h_5 = $2n+1$), the possible five-dimensional space group is centrosymmetric $P10_5/mmc$ or non-centrosymmetric $P10_5mc$. In this study, the former is assumed. The space group $P10_5/mmc$ is generated by a tenfold screw axis $\{C_{10} \mid \mathbf{d}_5/2\}$, a glide plane $\{\sigma \mid \mathbf{d}_5/2\}$ parallel to it, the inversion operation $\{I \mid 0\}$ and lattice translations $\{E \mid \mathbf{d}_i\}$ (i = 1, 2, ..., 5). The generators for this space group in the format of *International Tables for X-ray Crystallography* (1962) are given by $-t$, $x+y+z+t$, $-x$, $-y$, $u+\frac{1}{2}$; $-t$, $-z$, $-y$, $-x$, $u+\frac{1}{2}$; $-x$, $-y$, $-z$, $-t$, $-u$ and lattice translation $1+x$, y, z, t, u *etc.*

3. Structure modeling

3.1. Occupation domains

Within the framework of the five-dimensional description of decagonal quasicrystals, an occupation domain is defined as a two-dimensional area in the internal space. There are several possible ways to define the occupation domain (Yamamoto,

1996). We choose a polygonal description of it, owing to its geometric simplicity and the ease of performing subdivision and parametrization for the least-squares fitting (Yamamoto, 1996).

To define an occupation domain, we use five vectors in the internal space defined by

$$\mathbf{v}_j = 2a/5^{1/2}(c_{2j}\,\mathbf{a}_3 + s_{2j}\,\mathbf{a}_4), \quad (j = 1, \ldots, 5), \tag{3}$$

where $2a/5^{1/2} \simeq 2.43$ Å in the present case. Each vector is parallel to one of the center-to-vertex vectors of a reference pentagon. The vector $\mathbf{v}_5$ is redundant, since it is expressed by a linear combination of the other four as

$$\mathbf{v}_5 = -\mathbf{v}_1 - \mathbf{v}_2 - \mathbf{v}_3 - \mathbf{v}_4. \tag{4}$$

The other $\mathbf{v}_j$ ($j = 1, 2, 3, 4$) are equal to $\mathbf{d}_j^i - \mathbf{v}_5$, where $\mathbf{d}_j^i$ is the internal space component of the decagonal lattice vectors $\mathbf{d}_j$ defined in (2). By using (3) as unit vectors, a jth corner vector of an occupation domain is expressed by $\mathbf{e}_j = (x_1, x_2, x_3, x_4, x_5)$. For further details, refer to the literature (Weber & Yamamoto, 1997). (External and internal components of a five-dimensional vector are denoted hereafter by the superscripts e and i.)

3.2. Point density

The density of quasicrystals is a fundamental quantity. Therefore, a model which cannot explain the observed density is considered as an unreliable model. The point density is an equivalent quantity to the density, since it is given by the observed density and the chemical composition of the quasicrystals. In the present case, from the density D_x = 3.94 Mg m^{-3} and the chemical composition $Al_{72}Ni_{20}Co_8$, the point density is $\rho' = 0.0661$ Å^{-3}.

On the other hand, the point density of a model is given by

$$\rho' = \Omega/V_{\rm cell},$$

where $\Omega = \sum_k \Omega_k$ is the summed area of the occupation domains Ω_k in the internal space and $V_{\rm cell} = \det|M_{ij}|$ is the unit-cell volume of the five-dimensional decagonal lattice.

3.3. Initial model

The Patterson function with only $h_1h_2h_3h_40$ reflections suggests that most atom positions projected along the c axis correspond to the vertices of the Penrose tiling with an edge length of $2a/5^{1/2} \simeq 2.43$ Å. As is well known, the vertices of the Penrose tiling are classified into four groups by the positions of the occupation domains in the four-dimensional space (Janssen, 1986; Ishihara & Yamamoto, 1988). They are pentagonal-shaped occupation domains A, B, C and D placed at $(i, i, i, i)/5$ ($i = 1, 2, 3, 4$). A and D or B and C are related by an inversion operation. B and C are τ times larger than A and D. Therefore, with the radii $2a/5^{1/2}$ of occupation domains for A, D and $\tau(2a/5^{1/2})$ for B, C, a Penrose tiling with an edge length of $2a/5^{1/2} \simeq 2.43$ Å is obtained (Yamamoto & Ishihara, 1988).

A five-dimensional structure model can be constructed on the basis of the occupation domains of the Penrose tiling as follows. By considering the double-layered structure of $Al_{72}Ni_{20}Co_8$ and the space group $P10_5/mmc$, the occupation domains A and B are placed at $(\frac{1}{5}, \frac{1}{5}, \frac{1}{5}, \frac{1}{5}, \frac{1}{4})$ and $(\frac{2}{5}, \frac{2}{5}, \frac{2}{5}, \frac{2}{5}, \frac{1}{4})$ in the five-dimensional decagonal lattice. The site symmetry of these positions is $5m$, so that the equivalent occupation domains, corresponding to D and C, are generated at $(\frac{4}{5}, \frac{4}{5}, \frac{4}{5}, \frac{4}{5}, \frac{3}{4})$ and $(\frac{3}{5}, \frac{3}{5}, \frac{3}{5}, \frac{3}{5}, \frac{3}{4})$, respectively. This structure gives a point density of 0.0509 Å^{-3}, which is much smaller than the observed value of 0.0661 Å^{-3} for real $Al_{72}Ni_{20}Co_8$ quasicrystals.

By adding trapezoids A' (D') around the A (D) domains as indicated in Fig. 2, the point density of the model can be increased without any short atomic distance less than 2.43 Å in a layer. This model gives a point density of 0.0703 Å^{-3}. A

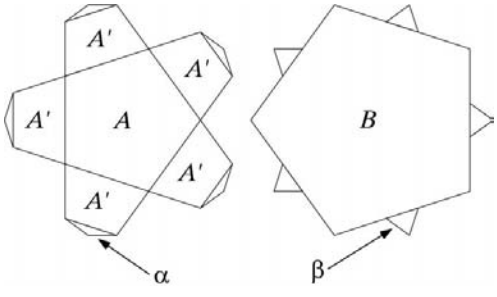

Figure 2
Occupation domains of an initial model for $Al_{72}Ni_{20}Co_8$ which are constructed on the basis of the Penrose tiling with an edge length of 2.43 Å.

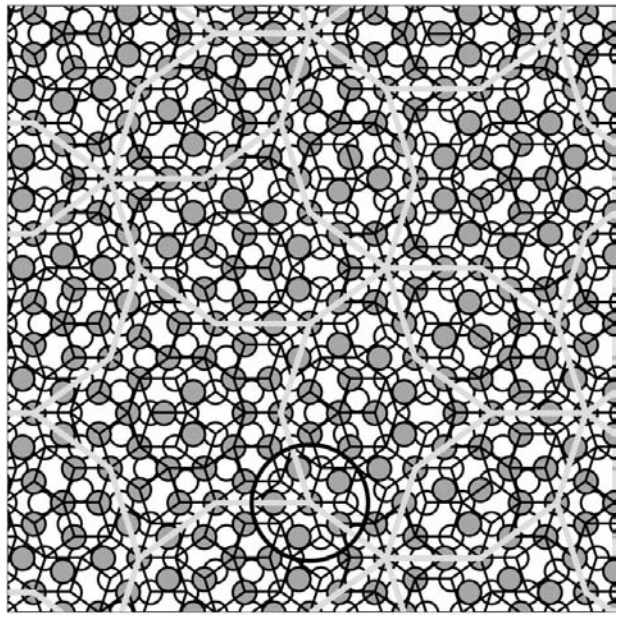

Figure 3
Projection of the atom positions (41 × 41 Å) created from the occupation domains in Fig. 2 along the c axis. The atoms at z = 0.25 and 0.75 are indicated by open and filled circles, respectively. The thin black lines show the Penrose tiling with an edge length of 2.43 Å. The thick grey lines indicate the hexagon, boat and star (HBS) tiling with an edge length of 6.36 Å. The thick black circle shows atom positions within a decagon of diameter 4.68 Å. They are located at the vertices of the HBS tiling (see text).

Table 1
Definitions of the independent subdomains used for constructing the large occupation domains in Fig. 4 (see text).

The superscript i refers to the internal space component. $\tau = (1 + 5^{1/2})/2$.

Symbol	Vectors			
a	$\mathbf{e}_1 = (\tau^{-2}, 0, 0, 0, 0)^i$	$\mathbf{e}_2 = (0, 0, 0, 0, -\tau^{-4})^i$	$\mathbf{e}_3 = (0, 0, 0, \tau^{-2}, 0)^i$	$\mathbf{e}_4 = (0, 0, -\tau^{-4}, 0, 0)^i$
	$\mathbf{e}_5 = (0, \tau^{-2}, 0, 0, 0)^i$	$\mathbf{e}_6 = (-\tau^{-4}, 0, 0, 0, 0)^i$	$\mathbf{e}_7 = (0, 0, 0, 0, \tau^{-2})^i$	$\mathbf{e}_8 = (0, 0, 0, -\tau^{-4}, 0)^i$
	$\mathbf{e}_9 = (0, 0, \tau^{-2}, 0, 0)^i$	$\mathbf{e}_{10} = (0, -\tau^{-4}, 0, 0, 0)^i$		
b	$\mathbf{e}_1 = (0, 0, 0, 0, -\tau^{-5})^i$	$\mathbf{e}_2 = (0, \tau^{-3}, 0, 0, 0)^i$	$\mathbf{e}_3 = (0, \tau^{-3}, \tau^{-3}, 0, 0)^i/2$	$\mathbf{e}_4 = (0, -\tau^{-5}, 0, 0, 0)^i$
c	$\mathbf{e}_1 = (\tau^{-3}, 0, 0, \tau^{-3}, 0)^i/2$	$\mathbf{e}_2 = (0, 0, 0, \tau^{-3}, 0)^i$	$\mathbf{e}_3 = (0, 0, 0, 0, \tau^{-3})^i$	$\mathbf{e}_4 = (\tau^{-3}, 0, 0, 0, 0)^i$
d	$\mathbf{e}_1 = (0, 0, 0, 0, -\tau^{-4})^i$	$\mathbf{e}_2 = (0, \tau^{-2}, 0, 0, 0)^i$	$\mathbf{e}_3 = (0, \tau^{-2}, \tau^{-2}, 0, 0)^i/2$	$\mathbf{e}_4 = (0, 0, \tau^{-2}, 0, 0)^i$
e	$\mathbf{e}_1 = (\tau^{-2}, 0, 0, \tau^{-2}, 0)^i/2$	$\mathbf{e}_2 = (0, 0, 0, \tau^{-2}, 0)^i$	$\mathbf{e}_3 = (0, 0, 0, 0, \tau^{-2})^i$	$\mathbf{e}_4 = (\tau^{-2}, 0, 0, 0, 0)^i$
f	$\mathbf{e}_1 = (\tau^{-3}, 0, 0, 0, 0)^i$	$\mathbf{e}_2 = (\tau^{-3}, 0, 0, \tau^{-3}, 0)^i/2$	$\mathbf{e}_3 = (0, 0, 0, \tau^{-3}, 0)^i$	$\mathbf{e}_4 = (0, \tau^{-3}, 0, \tau^{-3}, 0)^i/2$
	$\mathbf{e}_5 = (0, \tau^{-3}, 0, 0, 0)^i$	$\mathbf{e}_6 = (0, \tau^{-3}, 0, \tau^{-3}, 0)^i/2$	$\mathbf{e}_7 = (0, 0, 0, 0, \tau^{-3})^i$	$\mathbf{e}_8 = (0, 0, \tau^{-3}, 0, \tau^{-3})^i/2$
	$\mathbf{e}_9 = (0, 0, \tau^{-3}, 0, 0)^i$	$\mathbf{e}_{10} = (\tau^{-3}, 0, \tau^{-3}, 0, 0)^i/2$		
g	$\mathbf{e}_1 = (0, -\tau^{-3}, -\tau^{-3}, 0, 0)^i/2$	$\mathbf{e}_2 = (0, 0, -\tau^{-3}, 0, 0)^i$	$\mathbf{e}_3 = (0, 0, 0, \tau^{-3}, 0)^i$	$\mathbf{e}_4 = (0, -\tau^{-3}, 0, 0, 0)^i$

characteristic of the structure is that there are many atom positions forming a regular pentagon of diameter 4.86 Å. However, the arrangement of atom positions in a layer contains several vacant sites surrounded by atom positions forming the regular decagon with 7.83 Å diameter. In order to fill such vacant sites, small occupation domains α and β have to be considered as indicated by arrows in Fig. 2. Consequently, the resultant point density of the model becomes 0.0736 Å^{-3}, which is much larger than the observed value. Atom positions created from the occupation domains in Fig. 2 are shown in Fig. 3.

It is considered that this model structure produces reasonable atomic sites of the decagonal $Al_{72}Ni_{20}Co_8$ quasicrystal without unphysical short atomic distances in a layer. Therefore, we take these occupation domains (Fig. 2) as an initial model for the subsequent structure refinement. Hereafter, the large occupation domains $(A + A' + \alpha)$ and $(B + \beta)$ in Fig. 2 are called OD1 and OD2, respectively. In the course of the structure refinement, some parts of OD1 and/or OD2 should be treated as fractional or empty occupation domains so as to reproduce the observed point density and chemical composition.

The shapes of the occupation domains of this initial model are similar to those of previously proposed models by Yamamoto *et al.* (1990) for $Al_{70}Ni_{10}Co_{20}$ and Saitoh *et al.* (1998) for $Al_{70}Ni_{20}Co_8$. It should be noted that the latter model was proposed for Al–Ni–Co having the same chemical composition as in the present study.

They also have close resemblance to the occupation domains of a model of the decagonal Al–Cu–Co quasicrystals proposed by Cockayne & Widom (1998) except for the central part of B. In their model, a small pentagonal part of the domain, inversion of B having a radius τ^{-2} times smaller, is removed. Then this pentagonal domain is placed at $(\frac{2}{5}, \frac{2}{5}, \frac{2}{5}, \frac{2}{5}, 0)$. [Note that a superficial difference from Cockayne & Widom (1998) is due to the difference of the coordinate systems.]

4. Structure refinement and results

The subdivision of a large occupation domain depends on what kind of cluster is postulated in the higher-dimensional description of quasicrystals. As already mentioned, we do not employ a symmetric cluster model in the present analysis. In this case, the partitioning of the large occupation domains OD1 and OD2 is somewhat arbitrary. Previous studies have repeatedly suggested that OD1 contains most of the transition-metal (TM) atoms (Ni and Co), and OD2 contains mostly Al atoms (Yamamoto *et al.*, 1990; Steurer *et al.*, 1993; Saitoh *et al.*, 1998). Moreover, recent more reliable experimental data strongly suggest that the arrangement of TM atoms actually follows the Penrose tiling, and the local environment of the TM atoms is similar to that seen in the $Al_{13}Fe_4$-type approximant crystals (Saitoh *et al.*, 1997). Hence, the employed partitioning of OD1 was motivated by its resemblance to the arrangement of TM atoms which is found in the approximant crystals as demonstrated by Saitoh *et al.* (1998). In contrast to TM atoms, the arrangement of Al atoms in the approximant crystals is highly distorted. This means that there is no reliable basis for the partitioning of OD2. We took some practical requests to partition OD2, *i.e.* the number of parameters must be reasonable to perform a least-squares refinement and the resultant refinement must converge. Therefore, OD2 was divided into more than ten independent subdomains having almost the same size. A small occupation domain for Al located at $(\frac{2}{5}, \frac{2}{5}, \frac{2}{5}, \frac{2}{5}, 0)$, which exists in the model for Al–Cu–Co (Cockayne & Widom, 1998), has also been considered. In this analysis, however, this kind of model has been excluded. It is hopeless to distinguish between Ni and Co atoms by the conventional X-ray diffraction technique. Thus,

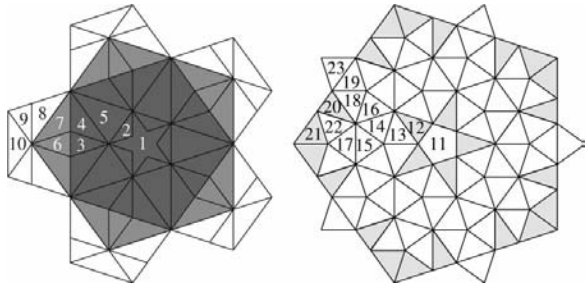

Figure 4
Final occupation domains as a result of the structure refinement of $Al_{72}Ni_{20}Co_8$. The darkness of the grey tone indicates the concentration of transition metals in the assigned small domains (see Table 2).

Table 2
Results of the structure refinement of a decagonal $Al_{72}Ni_{20}Co_8$ quasicrystal.

The symbol of the subdomains defined in Table 1 is given in column 2. Column 3 defines their internal space shift vectors from the center $\mathbf{x}_0$. Therefore, the actual position of the subdomains is $\mathbf{x}_0 + \mathbf{x}^i$. Column 4 gives the magnitudes, u_1 and u_2, of the displacement in the plane normal to the tenfold axis in the external space. Column 5 defines their shift vectors $\mathbf{x}_1^e$ and $\mathbf{x}_2^e$. (The superscripts i and e refer to the vector components in the internal and external space, respectively.) The final position of the subdomains is then given by $\mathbf{x} = \mathbf{x}_0 + \mathbf{x}^i + u_1[\mathbf{x}_1^e/|\mathbf{x}_1^e|] + u_2[\mathbf{x}_2^e/|\mathbf{x}_2^e|]$. Columns 6 and 7 give the isotropic and anisotropic a.d.p.s b_e and b_1, respectively. [For the definition of b_e and b_1, see text]. Column 8 gives the occupancy probability p of the subdomain. Column 9 gives the concentration probability s_1 of the transition metals (TM). The final column shows the name of the dominant element assigned in Fig. 4. In addition to the listed values, a phason displacement parameter $b_i = 1.583$ (4) (Å^2) was refined for all subdomains. An e.s.d. of less than 0.001 is indicated by †. $\alpha = \tau^{-1} = 0.618$, $\beta = \tau^{-2} = 0.382$, $\gamma = \tau^{-3} = 0.236$, $\delta = \tau^{-4} = 0.149$.

No.	Pre-OD	$\mathbf{x}^i$	u_1 (Å) u_2 (Å)	$\mathbf{x}_1^e$ $\mathbf{x}_2^e$	b_e (Å^2)	b_1 (Å^2)	p	s_1	Elements
OD1: $\mathbf{x}_0$ = (0.2, 0.2, 0.2, 0.2, 0.25)									
1	*a*	$(0, 0, 0, 0, 0, 0)^i$	– –	– –	0.643 (1)	−0.514 (12)	1.00 (–)	0.82 (1)	TM
2	*b*	$(0, 0, 0, 0, \gamma, 0)^i$	0.069 (1) –	$(0, 0, 0, 0, 1, 0)^e$ –	0.412 (1)	−0.101 (2)	1.00 (–)	0.99 (1)	TM
3	*c*	$(0, 0, 0, 0, -\alpha, 0)^i$	0.153 (1) –	$(0, 0, 0, 0, -1, 0)^e$ –	0.170 (2)	−0.172 (2)	1.00 (–)	1.00 (1)	TM
4	*d*	$(0, 0, \alpha, 0, \gamma, 0)^i$	−0.125 (†) 0.012 (†)	$(0, 0, 1, 0, 0, 0)^e$ $(0, 0, 0, 0, 1, 0)^e$	0.280 (1)	0.051 (1)	1.00 (–)	1.00 (1)	TM
5	*e*	$(0, 0, 0, 0, \alpha, 0)^i$	0.084 (†) –	$(0, 0, 0, 0, 0, 0)^e$ –	0.402 (1)	−0.240 (1)	1.00 (–)	1.00 (1)	TM
6	*c*	$(0, 0, 0, 0, -1, 0)^i$	0.208 (†) –	$(0, 0, 0, 0, 0, 0)^e$ –	0.192 (†)	−0.194 (†)	1.00 (–)	0.58 (1)	TM/Al
7	*d*	$(0, 0, \beta, 0, 2\beta, 0)^i$	−0.216 (†) –	$(0, 0, 0, 0, 0, 0)^e$ –	0.585 (3)	−0.264 (4)	1.00 (–)	0.49 (1)	TM/Al
8	*d*	$(0, 0, \beta, 0, 1, 0)^i$	−0.089 (†) −0.255 (†)	$(0, 0, 1, 0, 0, 0)^e$ $(0, 0, 0, 0, 1, 0)^e$	2.129 (14)	0.179 (4)	1.00 (–)	−0.01 (1)	Al
9	*c*	$(0, 0, -1-\gamma, 0, -\gamma, 0)^i$	0.452 (†) 0.776 (†)	$(0, 0, 0, -1, 0, 0)^e$ $(0, 0, 0, 0, -1, 0)^e$	1.192 (1)	−0.198 (7)	0.397 (1)	0.00 (1)	Al
10	*d*	$(0, 0, 0, 0, -1-\gamma, 0)^i$	−0.109 (†) –	$(0, 0, 0, 0, -1, 0)^e$ –	2.775 (9)	2.488 (8)	0.815 (†)	0.00 (1)	Al
OD2: $\mathbf{x}_0$ = (0.4, 0.4, 0.4, 0.4, 0.25)									
11	*f*	$(0, 0, 0, 0, 0, 0)^i$	– –	– –	5.042 (†)	5.042 (†)	0.50 (–)	0.00 (–)	Al
12	*c*	$(0, 0, 0, 0, \beta, 0)^i$	0.003 (†) –	$(0, 0, 0, 0, 1, 0)^e$ –	4.648 (1)	0.382 (5)	1.00 (–)	0.23 (1)	Al/TM
13	*g*	$(0, 0, 0, -\gamma, -\alpha, 0)^i$	−0.042 (1) −0.127 (†)	$(0, 0, 0, -1, 0, 0)^e$ $(0, 0, 0, 0, -1, 0)^e$	3.109 (9)	−2.562 (4)	1.00 (–)	0.00 (1)	Al
14	*g*	$(0, 0, -\gamma, 0, -\alpha, 0)^i$	0.018 (1) 0.102 (1)	$(0, 0, -1, 0, 0, 0)^e$ $(0, 0, 0, 0, -1, 0)^e$	2.343 (†)	−2.344 (†)	1.00 (–)	0.00 (1)	Al
15	*g*	$(0, 0, 0, 0, -\alpha-\gamma, 0)^i$	−0.068 (†) –	$(0, 0, 0, 0, -1, 0)^e$ –	2.272 (†)	−2.273 (†)	0.820 (1)	0.00 (1)	Al
16	*g*	$(0, 0, 0, \gamma, 1, 0)^i$	−0.208 (†) −0.053 (†)	$(0, 0, 0, 1, 0, 0)^e$ $(0, 0, 0, 0, 1, 0)^e$	2.270 (†)	−2.271 (†)	1.00 (–)	−0.01 (1)	Al
17	*g*	$(0, 0, 0, 0, -1, 0)^i$	−0.137 (†) –	$(0, 0, 0, 0, -1, 0)^e$ –	2.272 (†)	−2.273 (†)	0.820 (1)	0.00 (1)	Al
18	*g*	$(0, 0, \gamma, 0, 1, 0)^i$	−0.198 (2) −0.063 (1)	$(0, 0, 1, 0, 0, 0)^e$ $(0, 0, 0, 0, 1, 0)^e$	6.019 (29)	−4.536 (32)	1.00 (–)	−0.01 (1)	Al
19	*g*	$(0, 0, 0, 0, 1+\gamma, 0)^i$	−0.126 (†) –	$(0, 0, 0, 0, 1, 0)^e$ –	2.173 (1)	−1.530 (4)	1.00 (–)	0.05 (1)	Al
20	*c*	$(0, \beta, 0, 0, 1, 0)^i$	0.425 (1) −0.315 (†)	$(1, 0, 0, 0, 0, 0)^e$ $(0, 0, 0, 0, 1, 0)^e$	2.027 (29)	0.720 (2)	1.00 (–)	0.19 (1)	Al/TM
21	*g*	$(\gamma, 0, 0, 0, -1-\gamma, 0)^i$	−0.118 (†) −0.024 (†)	$(1, 0, 0, 0, 0, 0)^e$ $(0, 0, 0, 0, -1, 0)^e$	2.417 (1)	−1.578 (1)	1.00 (–)	0.23 (1)	Al/TM
22	*g*	$(0, 0, \gamma, 0, -1-\gamma, 0)^i$	0.100 (†) 0.065 (†)	$(0, 0, 1, 0, 0, 0)^e$ $(0, 0, 0, 0, -1, 0)^e$	2.032 (†)	−2.034 (†)	1.00 (–)	0.00 (1)	Al
23	*g*	$(0, 0, 0, 0, 1+\beta, 0)^i$	−0.102 (†) –	$(0, 0, 0, 0, 1, 0)^e$ –	2.173 (1)	−1.530 (4)	1.00 (–)	0.05 (1)	Al

the practical structure refinements were performed on a pseudo Al–TM binary system. For this purpose, a weighted atomic form factor for the TM (Ni:Co = 5:2) was used.

After various modifications in partitioning of the initial occupation domains OD1 and OD2 by taking into account the above consideration, we finally obtain $wR = 0.045$ [the weighting scheme is $w = 1/\sigma^2(|F_o|)$] and $R = 0.063$ for 103 refined parameters with 449 unique reflections. The final occupation domains are illustrated in Fig. 4. They are constructed by seven subdomains defined in Table 1. There are 23 independent subdomains defined in Table 2, for each of which the shift of the atom positions in the external space from their initial positions, phonon and phason displacement parameters, and occupation probability are defined, analo-

gously to Weber & Yamamoto (1997). As the phonon displacement parameter, we use b_e and b_1 to describe its anisotropy, which are defined by $B_\parallel = b_e + b_1$, $B_\perp = b_e - b_1$. $B_\parallel$ and $B_\perp$ represent a component of the anisotropic displacement parameter parallel to the quasiperiodic layer and along the tenfold axis. Therefore, b_e and b_1 represent the isotropic and anisotropic parts of the anisotropic displacement parameter.

The subdomains #9, #10, #11, #15 and #17 are treated as partially occupied ones. Of these, #11 was fixed at 0.5. Moreover, the subdomains #15 and #17 were grouped in terms of displacement parameter and occupancy probability factor. Such subdivisions enable the model to have positional shifts leading to asymmetric clusters. The quality of the final least-squares fit for the refinement is seen in Fig. 5.

In Table 2, refined parameters are listed. In addition to the parameters in Table 2, a phason isotropic displacement parameter, which is common to all small domains, was refined to be b_i = 1.583 (Å^2). Moreover, one scale factor and two parameters for the secondary-extinction factor are included. A strong 00002 reflection was not used for the least-squares refinement, since it was suspected of suffering a strong extinction effect. The weights for the three penalty functions, PF_1 for the occupation probabilities, PF_2 for the displacement parameters and PF_3 for the chemical composition, were chosen to be 0.5, 0.3 and 0.3, respectively [the definition of these constraints is referred to by Weber & Yamamoto (1997)]. The point density of the present model is 0.0686 Å. The refined chemical composition is $Al_{71.2}TM_{28.8}$. From these values, one obtains D_c = 4.12 Mg m^{-3}. The difference Fourier map showed maximum and minimum residual electron densities of $\Delta\rho_{max}$ = 2.99 Å^{-3} and $\Delta\rho_{min}$ = −0.77 Å^{-3}, respectively.

The above result is compared with those of previous studies. The structure analysis of $Al_{70}Ni_{10}Co_{20}$ quasicrystals reported R = 0.110 for the refinement with the overall isotropic phonon displacement parameter by using 41 strong reflections (Yamamoto *et al.*, 1990). Steurer *et al.* (1993) obtained wR = 0.078 and R = 0.091 for 21 refined parameters and 253 reflections for $Al_{70}Ni_{15}Co_{15}$ quasicrystals. In the present study, wR = 0.027 and R = 0.023, and wR = 0.037 and R = 0.041 were obtained for subsets of 100 and 300 strong reflections, respectively.

Besides the above analysis, we also performed structural refinements based on the Burkov model (Burkov, 1991) for the sake of comparison. This model is the prototype of a structure model consisting of 20 Å tenfold symmetric clusters. The original Burkov model has a large point density of 0.0736 Å^{-3}. Therefore, some occupation probabilities of the subdomains were also included as fitting parameters in the refinement. This model gave rather poor results of wR = 0.161 and R = 0.193 for 55 refined parameters with 10 independent subdomains. The refined point density was 0.0693 Å^{-3}, and the chemical composition was $Al_{64.9}TM_{35.1}$. The resultant calculated density was 4.39 Mg m^{-3}.

From these comparisons, it is confirmed that the present analysis provides much more accurate results than the previous ones.

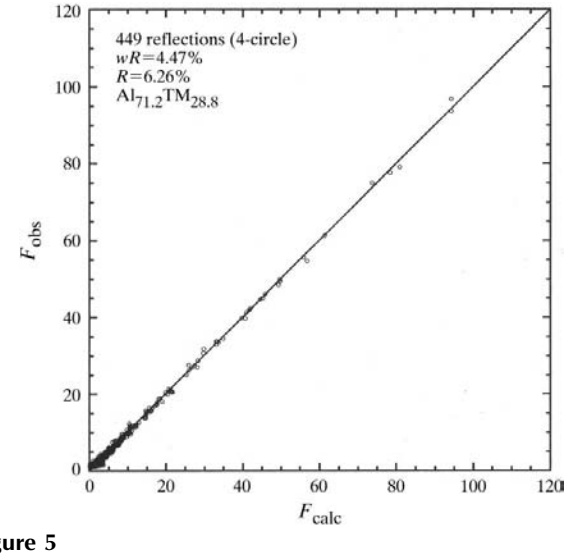

Figure 5
F_{obs}/F_{calc} plot for the final model of $Al_{72}Ni_{20}Co_8$.

5. Real-space structure of $Al_{72}Ni_{20}Co_8$

5.1. Layer structures

Fig. 6 shows a layer structure at z = 1/4 (fifth coordinate) obtained by an irrational cut of the refined five-dimensional structure in the external space. Here we concentrate on the

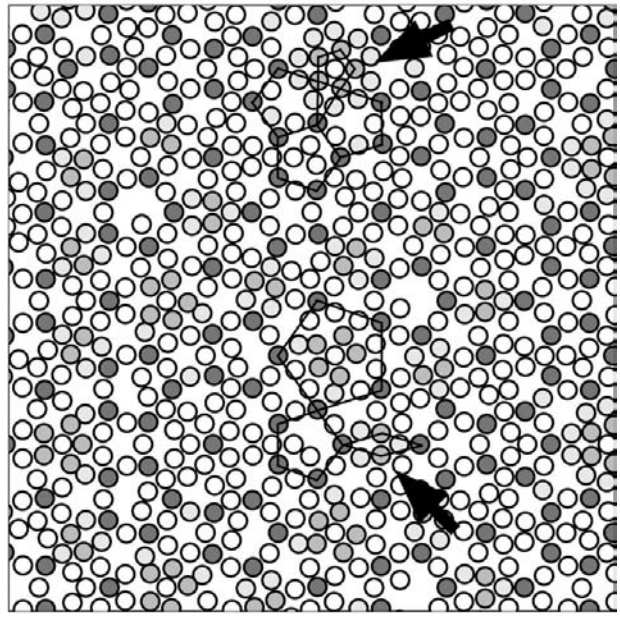

Figure 6
Layer structure (67 × 67 Å) at z = 1/4 of the refined structure of $Al_{72}Ni_{20}Co_8$. The filled circles with dark, middle and light grey tones correspond to TM, TM/Al and Al/TM atoms, respectively, coming from the assigned subdomains in Table 2. The open circles indicate Al atoms. The black lines indicate the connections between TM atoms having distances of 2.56, 4.76 and 7.46 Å.

arrangement of TM atoms which are indicated by grey tones in the figure. Connections between TM atoms are also indicated by black lines. There are many pentagonal motifs for TM atoms whose edge lengths are 2.56, 4.76 and 7.46 Å. The second and third lengths frequently appear in the monoclinic approximants of $A_{13}Fe_4$ and $A_{13}Co_4$ (Black, 1955*a*,*b*). This indicates a similarity of local arrangement of the TM atoms between the decagonal Al–Ni–Co quasicrystals and their approximant crystals. The length 2.56 Å is too short as a TM–TM distance. However, this length can be recognized as a TM–Al distance, since the corresponding atom sites which come from subdomains #6 and #7 are statistically occupied by TM and Al (see Table 2). In this respect, it is interesting to note that the location of such TM/Al sites appear as a group of short atomic distance sites as indicated by arrows in Fig. 6.

The other layer located at $z = 3/4$ has the same structure except for the orientation, *i.e.* the distribution of atoms in this layer is related to that of the layer at $z = 1/4$ by a tenfold screw axis in five-dimensional space.

5.2. Projected structure

Projections of the structure along the *c* axis are shown in Fig. 7. As seen in Table 2 and Fig. 7(*b*), all atoms show only small shifts from their initial (ideal) positions. In particular, the smallness in the shifts is remarkable for TM atoms. This indicates the validity of the initial model (Fig. 2), which is constructed from the Penrose tiling with an edge length of 2.43 Å. However, relatively large shifts are observed for atoms coming from subdomain #9. This seems to be attributable to inadequate parameterization of the Al atom positions by the current partitioning of the large occupation domains. It is also noticeable that a small occupancy probability of 0.4 was assigned to this subdomain.

The arrangement of atoms and their assignment of atomic species in Fig. 7 are inconsistent with the 20 Å tenfold symmetric cluster. It can be considered as an atomic decoration of the HBS tiling (Li, 1995) with an edge length of 6.36 Å. The 20 Å cluster region corresponds to a combination of two hexagons and one boat. This clearly reveals a symmetry breaking at the center of the 20 Å cluster. The vertices of the HBS tiling are mainly occupied by Al atoms and its edges by a pair of TM and TM/Al atoms. The latter is considered as a simple realisation of the matching rule for the Penrose tiling.

6. Discussion

The projected structures in Fig. 7 can be compared with images observed by electron microscopy. Previous structural studies of decagonal quasicrystals, mostly based on the HRTEM images, established the existence of the so-called 20 Å tenfold symmetric cluster. In the case of decagonal Al–Ni–Co quasicrystals, several studies have been performed for samples with a somewhat different composition, *e.g.* $Al_{70}Ni_{15}Co_{15}$ (Hiraga *et al.*, 1991). Although structure analyses of decagonal Al–Ni–Co quasicrystals have already shown some evidence of symmetry breaking of the 20 Å clusters (Steurer *et al.*, 1993), this point, as yet, has not been discussed further.

Furthermore, the HAADF images of the decagonal phase with composition $Al_{72}Ni_{20}Co_8$ have been observed recently (Saitoh *et al.*, 1997; Yan *et al.*, 1998). These images directly show the atomic positions of mainly TM atoms since the scattering power of the TM atoms is five times larger than that of Al atoms, and proved a symmetry breaking of the 20 Å clusters. Another investigation on the same material using HRTEM has also confirmed a triangular pattern in the center of the cluster (Abe *et al.*, 2000) that is not consistent with the perfect tenfold symmetry. The Fourier map is shown in Fig. 8. This can be compared with a HRTEM structure image [Fig. 2(*a*) of Abe *et al.* (2000)].

Two different models, however, have been proposed for almost the same HAADF images of $Al_{72}Ni_{20}Co_8$. One is based on a cluster constructed on the basis of its resemblance to a cluster found in the $Al_{13}Fe_4$-type approximant crystals (Saitoh *et al.*, 1998). This gives an interpretation for an intrinsic

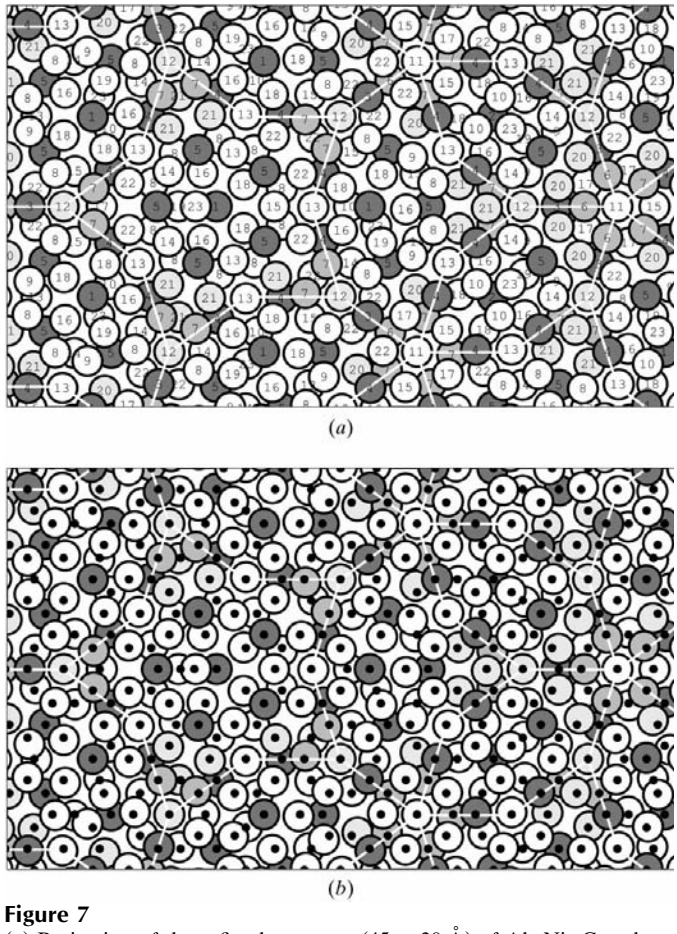

Figure 7
(*a*) Projection of the refined structure (45 × 30 Å) of $Al_{72}Ni_{20}Co_8$ along the *c* axis. The numbers indicate that atoms come from the small occupation domains with the same number in Fig. 4. The darkness of the grey tone indicates the concentration of transition metals in the assigned small domains in Table 2. The white lines indicate the HBS tiling with an edge length of 6.36 Å. (*b*) The same projected structure as (*a*), but the initial (ideal) atomic positions are indicated by small solid dots.

symmetry breaking of the 20 Å cluster. The other is based on the longly believed 20 Å cluster model with perfect tenfold symmetry (Yan *et al.*, 1998), *i.e.* the Burkov model (Burkov, 1991). In the latter, the appearance of the symmetry breaking is regarded as an accidental chemical ordering of TM and Al atoms at the center of the cluster, since the symmetry breaking cannot be described by the original Burkov model. The difference in the structure models my be attributed to the fact that diverse interpretations are possible for electron microscopy images, and such models are difficult to evaluate quantitatively from the images. The structure refinements as performed in the present study can only provide a statistically averaged structure in the five-dimensional space. Therefore, if the symmetry breaking of the cluster is an accidental one, the structure ought to be described by a model based on tenfold symmetric clusters. The poor fit with the Burkov model indicates that even an averaged structure of $Al_{72}Ni_{20}Co_8$ cannot be described with this model. It is thus considered that the symmetry breaking of the cluster is an intrinsic structural characteristic of the decagonal $Al_{72}Ni_{20}Co_8$ quasicrystals.

The present results fundamentally support the model proposed by Saitoh *et al.* (1998). However, there are still a few more discrepancies, as follows. In this model, clusters named S (star shape) are located at the vertices of the HBS tiling and the center of the cluster is assigned to a TM atom. The vertices of the HBS tiling come from subdomains #11, #12 and a part of #13 in Fig. 4. As seen in Fig. 4, only a small concentration (23%) of TM atoms is given by #12 and other domains are completely occupied by Al atoms in contrast to their assignment. Moreover, in our refined model, #6 and #7 are occupied by TM/Al atoms, while Saitoh *et al.* (1998) assigned them as Al atoms. As pointed out by Wittmann (1999), TM atoms in the HAADF images show elongated shapes and such a feature cannot be explained by the model proposed by Saitoh *et al.* (1998). Yan *et al.* (1998) resolved these elongated shapes and interpreted them as zigzag chains of TM atoms along the *c* axis. In the present refined structure, this is explained simply by a pair of TM and TM/Al atoms located on the edges of the HBS tiling with an edge length of 6.36 Å, which comes from a pair of subdomains #3 and #6 or #4 and #7 (Figs. 4 and 7). Therefore, the refined model is fully consistent with the observed HAADF images.

As a result, our refined structure model of the decagonal $Al_{72}Ni_{20}Co_8$ quasicrystal is very similar to a structure model of decagonal Al–Cu–Co quasicrystals proposed by Cockayne & Widom (1998), which has been constructed on the basis of Monte Carlo simulations. The distribution of Co atoms in their model almost corresponds to that of TM atoms in our model, and Cu atoms correspond to TM/Al atoms, respectively. It is also noted that their model was also interpreted by the HBS tiling with the same edge length of 6.36 Å.

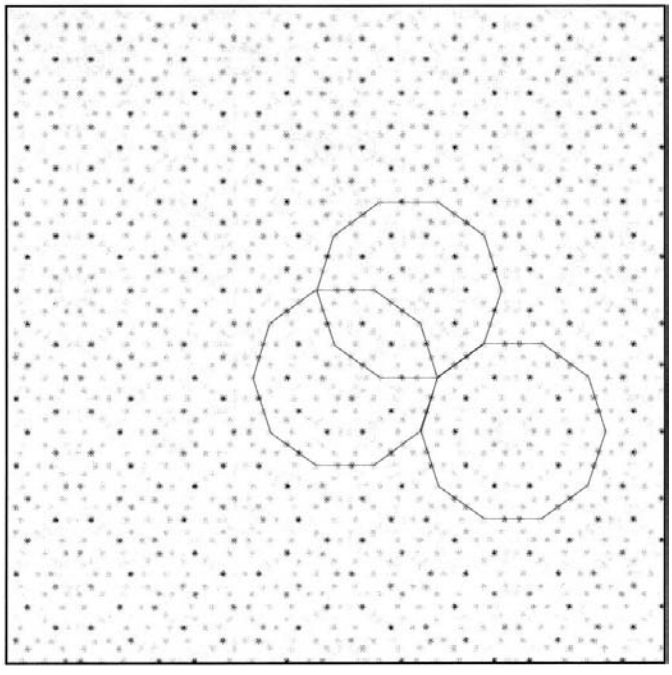

Figure 8
Fourier map (67 × 67 Å) in the external space for $Al_{72}Ni_{20}Co_8$ obtained from the $h_1h_2h_3h_40$ reflections only.

7. Conclusions

In this paper, we have described the results of a quantitative X-ray structure analysis performed on a single-crystal sample of decagonal $Al_{72}Ni_{20}Co_8$ quasicrystals. In spite of the assumptions made, the present study has shown that the structure of decagonal $Al_{72}Ni_{20}Co_8$ quasicrystals can be fitted with a five-dimensional cluster model that is not based on the 20 Å tenfold symmetric cluster motif which was believed to exist so far. The best-fit model gives a good agreement between observed and calculated diffraction intensities, with wR = 0.045 and R = 0.063 for 449 reflections with 103 parameters.

Several structure models proposed previously have been discussed in some detail. Then we have shown that the best-fit model can be regarded as a simple decoration of the HBS tiling with an edge length of 6.36 Å. The results obtained in the present study are very consistent with recent observations of this decagonal quasicrystal by high-resolution electron microscopy. It is expected that some further improvement, particularly in the calculated chemical composition and density, could be obtained by using even larger numbers of reflections in the refinement together with a more detailed partitioning of the occupation domains based on the present model.

Finally, the present study has shown that the structure refinement of quasicrystals with a higher-dimensional cluster model can be substantially improved by a parameterization based on a fine partitioning of the occupation domains. This kind of refinement could not be performed so far due to the imperfection of the quasicrystal sample itself. This analysis will be applicable to a wide range of quasicrystal structures if samples of sufficiently high quality are available as demonstrated in the present study.

The authors would like to thank Akira Sato, NIRIM, for technical support on the X-ray intensity data collection. One of the authors (HT) thanks Eiji Abe, NRIM, for stimulating discussions.

References

Abe, E., Saitoh, K., Takakura, H., Tsai, A. P., Steinhardt, P. J. & Jeong, H. C. (2000). *Phys. Rev. Lett.* **84**, 4609–4612.

Bendersky, L. (1985). *Phys. Rev. Lett.* **55**, 1461–1463.

Black, P. J. (1955*a*). *Acta Cryst.* **8**, 43–48.

Black, P. J. (1955*b*). *Acta Cryst.* **8**, 175–182.

Burkov, S. E. (1991). *Phys. Rev. Lett.* **67**, 614–617.

Chattopadhyay, K., Lele, S., Ranganathan, S., Subbanna, G. N. & Thangaraj, N. (1985). *Curr. Sci.* **54**, 895–903.

Cockayne, E. & Widom, M. (1998). *Phys. Rev. Lett.* **81**, 598–601.

Edagawa, K., Ichihara, M., Suzuki, K. & Takeuchi, S. (1992). *Philos. Mag. Lett.* **66**, 19–25.

Edagawa, K., Sawa, H. & Takeuchi, S. (1994). *Philos. Mag. Lett.* **69**, 227–234.

Frey, F., Weidner, E., Hradil, K., Boissieu, M. D., Currat, R., Shibata, K., Tsai, A. P. & Sato, T. J. (2000). *Philos. Mag. A*, **80**, 2375–2391.

Gödecke, T. & Ellner, M. (1996). *Z. Metallkd.* **87**, 854–864.

Gödecke, T. & Ellner, M. (1997). *Z. Metallkd.* **88**, 382–389.

Gummelt, P. (1996). *Geometriae*, **62**, 1–17.

Hiraga, K., Sun, F. J. & Sun, W. (1991). *Mater. Trans. Jpn. Inst. Met.* **32**, 308–314.

International Tables for X-ray Crystallography (1962). Vol. III. Birmingham: Kynoch Press.

Ishihara, K. N. & Yamamoto, A. (1988). *Acta Cryst.* A**44**, 508–516.

Janssen, T. (1986). *Acta Cryst.* A**42**, 261–271.

Li, X. Z. (1995). *Acta Cryst.* B**51**, 265–270.

Ritsch, S., Beeli, C., Nissen, H. U., Gödecke, T., Scheffer, M. & Lück, R. (1996). *Philos. Mag. Lett.* **74**, 99–106.

Ritsch, S., Beeli, C., Nissen, H. U., Gödecke, T., Scheffer, M. & Lück, R. (1998). *Philos. Mag. Lett.* **78**, 67–75.

Ritsch, S., Beeli, C., Nissen, H. U. & Lück, R. (1995). *Philos. Mag. A*, **71**, 671–685.

Saitoh, K., Tsuda, K. & Tanaka, M. (1998). *J. Phys. Soc. Jpn*, **67**, 2878–2581.

Saitoh, K., Tsuda, K., Tanaka, M., Kaneko, K. & Tsai, A. P. (1997). *Jpn. J. Appl. Phys.* **36**, L1400–L1402.

Scheffer, M., Gödecke, T., Lück, R., Ritsch, S. & Beeli, C. (1998). *Z. Metallkd.* **89**, 270–278.

Shechtman, D., Blech, I., Gratias, D. & Chan, J. W. (1984). *Phys. Rev. Lett.* **53**, 1951–1953.

Steinhardt, P. J., Jeong, H. C., Saitoh, K., Tanaka, M., Abe, E. & Tsai, A. P. (1998). *Nature (London)*, **396**, 55–57.

Steurer, W., Haibach, T., Zhang, B., Kek, S. & Lück, R. (1993). *Acta Cryst.* B**49**, 661–675.

Tsai, A. P. (1999). *Metallurgy of Quasicrystals*, in *Physical Properties of Quasicrystals.* Berlin: Springer-Verlag.

Tsai, A. P., Fujiwara, A., Inoue, A. & Masumoto, T. (1996). *Philos. Mag. Lett.* **74**, 223–240.

Tsai, A. P., Inoue, A. & Masumoto, T. (1989). *Mater. Trans. Jpn. Inst. Met.* **30**, 463–473.

Weber, S. & Yamamoto, A. (1997). *Philos. Mag. A*, **76**, 85–106.

Weber, S. & Yamamoto, A. (1998). *Acta Cryst.* A**54**, 997–1005.

Wittmann, R. (1999). *Z. Kristallogr.* **214**, 501–505.

Yamamoto, A. (1996). *Acta Cryst.* A**52**, 509–560.

Yamamoto, A. & Ishihara, K. N. (1988). *Acta Cryst.* A**44**, 707–714.

Yamamoto, A., Kato, K., Shibuya, T. & Takeuchi, S. (1990). *Phys. Rev. Lett.* **65**, 1603–1606.

Yamamoto, A., Sato, A., Kato, K., Tsai, A. P. & Masumoto, T. (1994). *Mater. Sci. Forum*, **150/151**, 211–222.

Yan, Y., Pennycook, S. J. & Tsai, A. (1998). *Phys. Rev. Lett.* **81**, 5145–5148.